PROCEEDINGS OF SCIENCE

Direct Measurement of QED Radiative Effects in PRad Experiment

Chao Peng[a,*] **and Dipangkar Dutta**[b]

[a] *Argonne National Laboratory, 9700 S Cass Ave, Lemont, IL, USA*

[b] *Department of Physics and Astronomy, Mississippi State University, Mississippi State, MS, USA*

E-mail: cpeng@anl.gov, d.dutta@msstate.edu

The PRad experiment at Jefferson Lab has precisely measured the cross sections for elastic electron-proton scattering at four momentum transfer square $2 \times 10^{-4} < Q^2 < 6 \times 10^{-2}$ GeV^2. The proton's charge radius was extracted based on the measured proton form factors at very low Q^2. This experiment utilized a high-precision, hybrid calorimeter (HyCal) to precisely determine the energy and position of electrons and photons. The HyCal's inner array of $PbWO_4$ modules can well separate two incident particles with a distance greater than about 30 mm (of the module size) on the detection plane. Together with the GEM detectors placed in front of the HyCal, which serve as a veto detector for neutral particles, the PRad detector system is capable of measuring and identifying the scattered electrons and the radiative photons simultaneously from the elastic ep and ee scattering processes. In this proceeding, the preliminary results of the direct radiative effects measurement from the PRad experiment are discussed; the expected improvements with the upcoming PRad-II experiment are also presented.

The XVIth Quark Confinement and the Hadron Spectrum Conference (QCHSC24)
19-24 August, 2024
Cairns Convention Centre, Cairns, Queensland, Australia

*Speaker

 ISSN 1824-8039 . Published by SISSA Medialab.

PoS(QCHSC24)072

1. Introduction

All electron scattering experiments must account for the fact that electrons radiate in the presence of nuclei or other electrons. Typically this radiation results in an unwanted background in the spectrum of the scattered electrons, and these radiative tails must be accurately calculated to extract any reliable information from electron scattering experiments. These so-called radiative corrections have a long history, starting with Schwinger's [1] calculation of the full first-order corrections to the spectrum of electrons scattering in a coulomb potential. They include vacuum polarization, vertex corrections, and internal Bremsstrahlung grouped as "internal corrections" as well as external Bremsstrahlung and ionization energy loss. However, individual photons can be emitted with arbitrarily small energies, making it impossible to completely specify all the final states of the system, leading to the infamous "infrared catastrophe" of lowest order perturbation theory [2]. The infrared divergence problem was solved by extending these calculations to higher orders and separating the divergences as multiplicative, exponential factors while converting the residual expansion to be divergence-free [3]. In the multiplicative infrared factors, the divergences from real and virtual photons cancel out, providing a powerful and accurate way of estimating radiative corrections in electron scattering. This procedure for canceling infrared divergences is also known as the BRS transformation.

Later, a review by Mo and Tsai [4] presented a comprehensive formulation for a set of approximations that could be used for radiative corrections of a wide range of electron scattering processes. It involves an arbitrary energy scale (typically chosen to be smaller than the experimental resolution) to separate between the "soft" and "hard" Bremsstrahlung. The "soft" photon emission is merged with the elastic process, and the "hard" Bremsstrahlung is exponentiated, assuming that if the photon energy is high enough, multi-photon emission is possible. The Mo and Tsai formulation has remained one of the most popular approaches to estimating radiative corrections in lepton scattering experiments. However, de Calan, Navelet, and Picard [5] have derived an alternate approach that disagrees by $> 20\%$ for inclusive scattering at a few GeV electron energies. This is an order of magnitude larger than the typical uncertainty quoted for the radiative correction procedures [5]. Modern radiative correction calculations have eliminated the ultra-relativistic approximation where the mass of the electron is neglected [6], some use an exact calculation of the next-to-leading order (NLO) internal Bremsstrahlung [7], and others include many next-to-next-to-leading order (NNLO) corrections [8]. However, they all rely on the Suura transformation inspired by the higher-order divergence cancellation scheme [3]. Under this scheme, even if the final correction is small, the first-order real and virtual corrections being merged can be large and therefore the uncertainty due to the scheme could be significantly larger than the final correction. The observed qualitative agreement between calculations and radiatively corrected spectra in electron scattering experiments is the only indirect validation of this procedure.

Since radiative corrections are an essential part of all electron scattering experiments, especially high precision ones, such as the proton charge radius experiment, PRad [9] and many others [10–12], it is of utmost importance to validate the best formulation through robust direct measurements. To date, there have been no direct measurements of the radiative photons for a clean validation of the radiative correction formulations. The closest direct evidence comes from $e-p$ deep inelastic scattering (DIS) measurements at the HERA collider. Radiative elastic ep events were detected

at very small angles ($\theta < 0.5$ mrad with respect to the electron beam) in dedicated calorimeters to monitor the luminosity of the beam [13]. However, this measurement lacked precision due to the difficulty of measuring low 4-momentum transfer squared (Q^2) processes in the beam colliding mode, and the large uncertainty of the electron beam tilt [13]. In this article, we describe the first direct measurement of radiative photons from $e-e$ collisions using a Hybrid calorimeter [14] called HyCal during the PRad experiment [9]. We have used the measured Bremsstrahlung photon yield buried under the $e-e$ peak and their angular distribution to validate the radiative correction procedure used in the PRad experiment [9].

2. The Experiment

The PRad collaboration at Jefferson Lab developed and performed a new $e-p$ experiment as an independent measurement of the proton charge radius (r_p) to address this "puzzle" [9]. The PRad experimental apparatus consisted of four elements (Figure 1): (i) a 4 cm long, cryo-

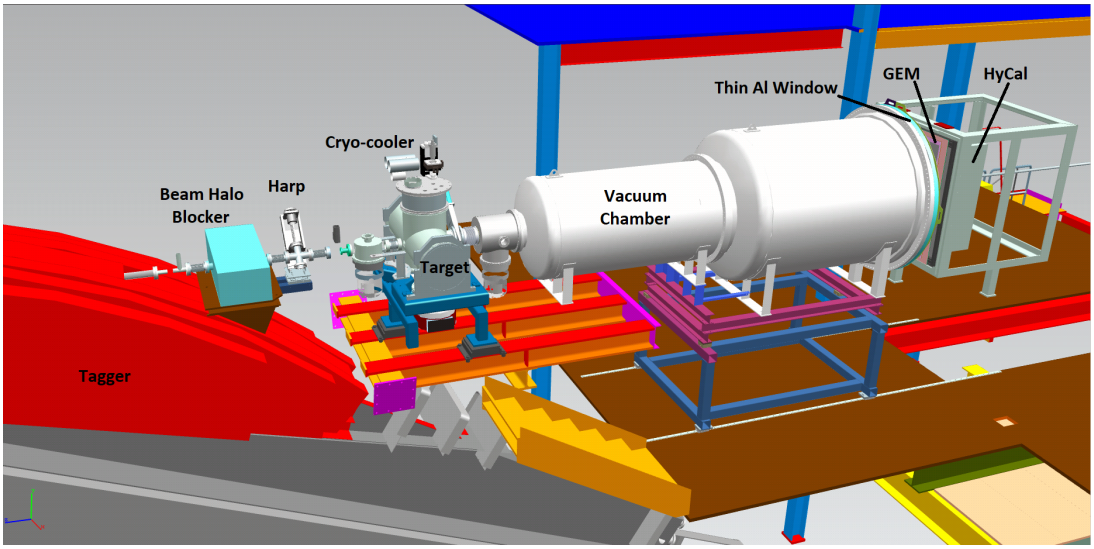

Figure 1: A schematic layout of the PRad experimental setup in Hall B at Jefferson Lab, with the electron beam incident from the left. The key beam line elements are shown along with the windowless hydrogen gas target, the two-segment vacuum chamber, and the two detector systems, GEM and HyCal.

cooled, windowless hydrogen (H_2) gas flow target with a density of 2×10^{18} atoms/cm^2; (ii) a high resolution, large acceptance HyCal electromagnetic calorimeter [14], which provides complete azimuthal coverage for the forward scattering angles and is able to simultaneously detect both electrons and photons from the radiative $e-p$ scattering; (iii) one tracking plane made of two high resolution $X-Y$ gas electron multiplier (GEM) coordinate detectors located in front of HyCal, and can be used to distinguish the photons from the electrons; and (iv) a two-section vacuum chamber spanning the 5.5 m distance from the target to the detectors.

The PRad experiment was performed in Hall B at Jefferson Lab using 1.101 GeV and 2.143 GeV continuous wave (CW) electron beams. The standard low beam current (0.1-50 nA) Hall B beamline was used in this experiment. The incident electrons that scattered off the target protons and the radiated hard photon were detected using the GEM and HyCal detectors. The PrimEx HyCal

calorimeter [14] is a hybrid electromagnetic calorimeter consisting of two different types of shower detectors, 576 Pb-glass modules ($3.82 \times 3.82 \times 45$ cm^3) and 1152 $PbWO_4$ crystal modules ($2.05 \times 2.05 \times 18.0$ cm^3). The calorimeter with its 116×116 cm^2 cross-sectional area was located in the beamline at a distance of 5.5 m from the hydrogen target. The $PbWO_4$ crystals were wrapped in 100 μm VM2000 reflective material to improve light collection and then in 36 μm of Tedlar for light isolation. The crystals were attached to Hamamatsu R4125HA photo-multiplier tubes with optical grease. The Pb-glass modules were wrapped in 25 μm aluminized mylar foil and the light was detected in Russian-made FEU 84-3 photo-multiplier tubes. The electron beam passed through a 4.0×4.0 cm^2 hole in the central part of HyCal (2×2 $PbWO_4$ modules are removed from the assembly). The gain stability of each channel is monitored using a blue LED-based light monitoring system (LMS).

A Gas Electron Multiplier (GEM) detector layer was located just in front of the calorimeter. The GEM layer was built to match the area of the calorimeter and was made of two large-area GEM detectors, each with an active area of 123 cm by 55 cm, arranged so that there is a narrow overlap area in the middle. A hole with a 4 cm diameter was built into the GEM detectors at the center of the active area allowing for the passage of the beamline. The GEM detectors were based on triple GEM foil structures followed by 2D x-y strip readout layers. Each pair of GEM foils had 2×4 grid of thin dielectric spacers between them to prevent them from coming into contact with each other. Each large-area GEM foil was subdivided into 60 high-voltage sectors, separated by 100 μm narrow gaps. The GEM efficiency loss due to the presence of the spacers and sector margins was measured using data and was modeled in the simulation.

The energy and position of the detected electron and photon were measured by HyCal, and the transverse ($X - Y$) position of the electron was measured by the GEM detector, which was used to assign the Q^2 for each detected event. The GEM detector was also used to distinguish between scattered electrons and photons. The GEM detector, with a position resolution of 72 μm, improved the accuracy of Q^2 determination because the HyCal is equally sensitive to electrons and photons while the GEM is mostly insensitive to neutral particles. The GEM detector also helped suppress the position-dependent irregularities in the response of the electromagnetic calorimeter.

A plot of the reconstructed energy versus the reconstructed angle for $e - p$ and $e - e$ events is shown in Figure 2 for the 2.2 GeV beam energy.

The background was measured periodically with an empty target cell. To mimic the residual gas in the beam line, H_2 gas at very low pressure was allowed in the target chamber during the empty target runs. The charge normalized $e - p$ and Møller yields from the empty target cell were used to effectively subtract the background contributions. The beam current was measured with the Hall-B Faraday cup with an uncertainty of $< 0.1\%$ [15].

A comprehensive Monte Carlo simulation of the PRad setup was developed using the Geant4 toolkit [16]. The simulation consists of event generators built for the $e-p$ and $e-e$ processes [6, 17], and they include next-to-leading order contributions to the cross-section (radiative corrections), such as Bremsstrahlung, vacuum polarization, self-energy, and vertex corrections. The calculations of the $e - p$ elastic radiative corrections are performed within a covariant formalism, without the usual ultra-relativistic approximation [6], where the mass of the electron is neglected. The generators also include contributions from two-photon exchange processes [18–20]. A second independent $e - p$ elastic event generator [17] was used as a cross-check. The radiative corrections to the proton,

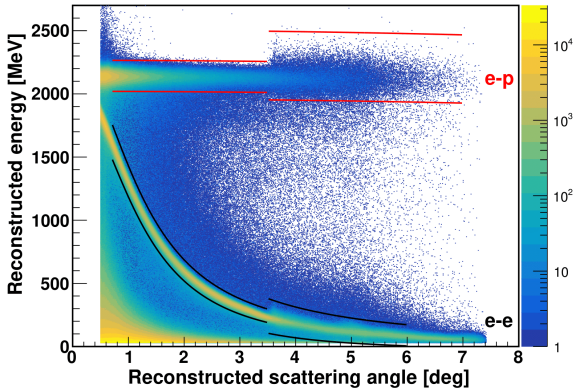

Figure 2: The reconstructed energy vs angle for $e-p$ and $e-e$ events for the electron beam energy of 2.143 GeV. The red and black lines indicate the event selection for $e-p$ and $e-e$, respectively. The angles $\leq 3.5°$ are covered by the $PbWO_4$ crystals and the rest by the Pb-glass part of HyCal.

which are typically neglected, were included in the alternate generator. The two $e-p$ generators were found to be in excellent agreement.

Inelastic $e-p$ scattering events were included in the simulation using an empirical fit [21] to the $e-p$ inelastic scattering world data. Inelastic $e-p$ scattering contributes a background to the $e-p$ elastic spectrum, which, when included in the simulation, was able to reproduce the measured elastic $e-p$ spectrum. The simulation included signal digitization and photon propagation, which were critical for the precise reconstruction of the position and energy of each event in the HyCal. Simulated charged particles with known energy and angles that produce a signal in the calorimeter were utilized to generate a collection of profiles of the signal as distributed among the calorimeter modules (cluster profiles). The simulated cluster profiles are compared with the cluster profiles for each detected event, where all the calorimeter modules with signal in a neighboring module were grouped together (also known as "island clustering"). Further, the clusters from detected events are iteratively subdivided until a best match is achieved with the simulated cluster profiles. The energy and position of each cluster is then determined from the center of gravity of the cluster with logarithmic weighting corresponding to the exponential decay of the signal strength with distance from the hit center. Corrections arising from the non-linear response of the calorimeter modules, and signal leakage at the gaps between the modules or at the detector boundaries were obtained from the calibration data and applied to the reconstructed energy and position. Finally, the reconstructed position of the event was substituted with the reconstructed position of the best-matching GEM hit within a coincidence time window of ~200 ns.

3. Direct Measurement of Radiative Photons

The window-less design of the PRad target ensured that there were negligible contributions to the background from initial state radiative photons originating from electrons interacting with materials other than the hydrogen atoms. The PRad detectors can identify photons by discarding all the clusters in the calorimeter that produce a signal in the GEM detector. Further, radiative photons were identified by their cluster-splitting pattern (*i.e.*, the presence of an adjoining second maxima

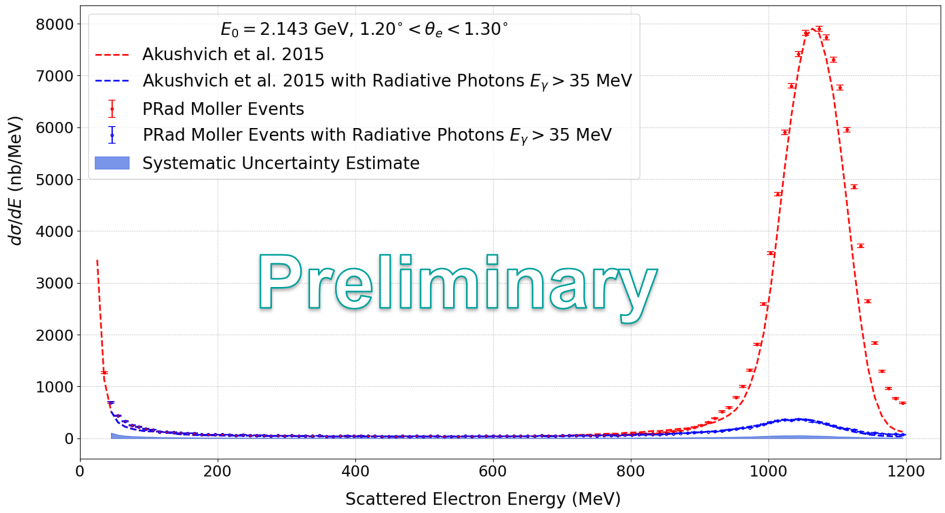

Figure 3: The cross section as a function of the reconstructed scattered electron energy for the $e-e$ events for an electron beam energy of 1.143 GeV. The red points are the events without radiative photons, and the blue points are events with radiative photons. The red solid curve and the blue dashed curves are the simulation results based on the radiative effects calculation from Akusevish *et al.* [6] without and with the radiative photon energy cut, respectively.

in the energy profile when the clusters were examined between two corners or between two sides. The radiative $e-e$ events were identified by the coincidence between two electrons and at least one radiative photon with constraints on the azimuthal angle to ensure co-planarity of the two electrons and constraints on the total energy to ensure elasticity. For the symmetric $e-e$ events, the electron scattering angle for each electron was restricted to $1.2 < \theta < 1.3$ degrees. The events impacted by the collimator's shielding the crystals closest to the beam, were also removed. Only the $e-e$ events with radiative photon energy $E_\gamma > 35$ MeV were selected. Given the large distance of 5.6 m between the target and the calorimeter, the minimum opening angle of the radiative photons was as low as 0.3°.

In Fig. 3, the $e-e$ cross section with and without the radiative photons (for $E_\gamma > 35$ MeV) is shown as a function of the scattered electron energy ($E^{'}$). The peak at $E^{'} \sim 1.1$ GeV corresponds to the elastically scattered electrons from the Møller process, while the rising curve at the lowest energies corresponds to the radiative tail. As expected, the radiative $e-e$ events are buried under the higher energy (small angle) $e-e$ peak, which cannot be separated without direct detection of the low-energy radiative photons. Both the energy distribution and the magnitude of the cross section with and without radiative photons agree well with the calculations of Akusevish *et al.* [6]. These calculations use a complete set of analytical expressions for electromagnetic radiative corrections to $e-e$ scattering obtained within a covariant formalism and beyond the ultra-relativistic approximation that is presented in Ref. [6]. They constitute the exact expressions for the radiative corrections to $e-e$ scattering, including all loops and the emission of additional real photons from each electron.

Through our studies with the PRad data, the efficiency of the radiative photon detection is

limited mostly by the single plane of the GEM-based coordinate detector. Therefore, the contamination from false-positively identified photons from the Møller process prevented us from extracting a similar cross-section spectrum of the radiative elastic $e - p$ process. However, future PRad-II experiments will have two GEM planes, and thus the upgraded detector system will allow better radiative photon detection. This will lead to more effective and precise studies of the radiative $e - p$ and Møller cross sections.

References

[1] Julian S. Schwinger. Quantum electrodynamics. III: The electromagnetic properties of the electron: Radiative corrections to scattering. *Phys. Rev.*, 76:790–817, 1949.

[2] F. Bloch and A. Nordsieck. Note on the Radiation Field of the electron. *Phys. Rev.*, 52:54–59, 1937.

[3] D. R. Yennie, Steven C. Frautschi, and H. Suura. The infrared divergence phenomena and high-energy processes. *Annals Phys.*, 13:379–452, 1961.

[4] Luke W. Mo and Yung-Su Tsai. Radiative Corrections to Elastic and Inelastic e p and mu p Scattering. *Rev. Mod. Phys.*, 41:205–235, 1969.

[5] Claude de Calan, Henri Navelet, and Jean Picard. Generalized radiative corrections for hadronic targets. *Nucl. Phys. B*, 348:47–65, 1991.

[6] I. Akushevich, H. Gao, A. Ilyichev, and M. Meziane. Radiative corrections beyond the ultra relativistic limit in unpolarized ep elastic and Møller scatterings for the PRad Experiment at Jefferson Laboratory,. *Eur. Phys. J. A*, 51:2015–15001, 2015.

[7] L. Li et al. Instrumental uncertainties in radiative corrections for the MUSE experiment. *Eur. Phys. J. A*, 60(1):8, 2024.

[8] P. Banerjee, T. Engel, A. Signer, and Y. Ulrich. QED at NNLO with McMule. *SciPost Phys.*, 9:027, 2020.

[9] W. Xiong et al. A small proton charge radius from an electron–proton scattering experiment. *Nature*, 575(7781):147–150, 2019.

[10] Y. Wang, J. C. Bernauer, B. S. Schlimme, P. Achenbach, S. Aulenbacher, M. Ball, M. Biroth, D. Bonaventura, D. Bosnar, P. Brand, S. Caiazza, M. Christmann, E. Cline, A. Denig, M. O. Distler, L. Doria, P. Eckert, A. Esser, I. Friščić, S. Gagneur, J. Geimer, S. Grieser, P. Gülker, P. Herrmann, M. Hoek, S. Kegel, J. Kelsey, P. Klag, A. Khoukaz, M. Kohl, T. Kolar, M. Lauß, L. Leßmann, M. Littich, S. Lunkenheimer, J. Marekovič, D. Markus, M. Mauch, H. Merkel, M. Mihovilovič, R. G. Milner, J. Müller, U. Müller, T. Petrovič, J. Pochodzalla, J. Rausch, J. Schlaadt, H. Schürg, C. Sfienti, S. Širca, R. Spreckels, S. Stengel, Y. Stöttinger, C. Szyszka, M. Thiel, S. Vestrick, and C. Vidal. Low-Q^2 elastic electron-proton scattering using a gas jet target. *Phys. Rev. C*, 106:044610, Oct 2022.

[11] A. Vorobyev. Precision measurement of the proton charge radius in electron proton scattering. *Phys. Part. Nucl. Lett.*, 16(5):524–529, 2019.

[12] Ethan Cline, Jan Bernauer, Evangeline J. Downie, and Ronald Gilman. MUSE: The MUon Scattering Experiment. *SciPost Phys. Proc.*, page 023, 2021.

[13] M. W. Krasny. Proceedings of the XXI International Meeting on Fundamental Physics, Madrid, Spain. page 210. World Scientific, 1993.

[14] A. Gasparian. Proc. XI Int. Conf. Calorim. Par. Phys. pages 109–115. World Scientific, Singapore, 2005.

[15] B. Mecking et al. The CEBAF large acceptance spectrometer (CLAS). *Nucl. Inst. and Meth. A*, 503:513–553, 2003.

[16] S. Agostinelli et al. GEANT4: A simulation toolkit. *Nucl. Inst. and Meth. A*, 506:250–303, 2003.

[17] A. V. Gramolin et al. A new event generator for the elastic scattering of charged leptons on proton. *J. Phys. G*, 41:115001, 2014.

[18] O. Tomalak. Two-photon exchange correction in elastic lepton-proton scattering. *Few Body Syst.*, 59:87, 2018.

[19] O. Tomalak and M. Vanderhaeghen. Two-photon exchange correction in elastic unpolarized electron-proton scattering at small momentum transfer. *Phys. Rev. D*, 93:013023, 2016.

[20] O. Tomalak and M. Vanderhaeghen. Subtracted dispersion relation formalism for the two-photon exchange correction to elastic electron-proton scattering: Comparison with data. *Eur. Phys. J. A*, 51:24, 2015.

[21] M.E. Christy and P.E. Bosted. Empirical fit to precision inclusive electron-proton cross-sections in the resonance region. *Phys. Rev. C*, 81:055213, 2010.